High-Dynamic and High-resolution Automatic Photon Counting OTDR for Optical Fiber Network Monitoring

Felipe Calliari[1], Luis E. Y. Herrera[1], Jean Pierre von der Weid[1] and Gustavo C. Amaral[1,2]
[1]*Center for Telecommunication Studies, Pontifical Catholic University of Rio de Janeiro, Rio de Janeiro 22451-900, Brazil*
[2]*Institute for Quantum Information Science, and Department of Physics and Astronomy, University of Calgary, Calgary, Canada*

Keywords: Photon-Counting OTDR, Signal Processing, FPGA.

Abstract: In this work, the development of a hybrid structure for the monitoring of optical fibers, using two types of Photon Counting Optical Time Domain Reflectometers (ν-OTDR), is presented. While one ν-OTDR presents a 32 dB dynamic range with spatial resolution of 6 m and minute-range measurements, the other has a 14 dB dynamic range and a resolution of 3 cm with hour-range measurements. By employing a trend filter capable of detecting fiber faults in the ν-OTDR fiber profile and interchanging between either OTDR techniques in an automatic fashion, we were able to harness the qualities of both in the minimum amount of measurement time. Our experimental results performed with multiple optical fiber links attest the structure's capability of automatically detecting faults in an optical fiber link with ultra-high-resolution and minute-range measurements. Furthermore, tunability of the hybrid structure enabling the monitoring of wavelength-division multiplexed optical networks has been demonstrated.

1 INTRODUCTION

Optical fibers have many advantages over other transmission methods (cables, satellites, etc.), which amounts to its immunity to electrical or magnetic interference, its weight in relation to metallic cables, and its low manufacturing cost. Although optical fibers are rather reliable, they can sometimes be damaged. The causes are the most varied: in the ocean, for example, ships can break optical fibers, and even sharks and other marine animals can chew the fiber protective coating. On land, optical fibers are used following physical infrastructures such as highways, railroads and electric power transmission lines and can be broken due to works, storms or accidents. In general, mechanical stress is highly prejudicial and should be avoided.

Fiber monitoring is essential to enable long-distance optical telecommunications links since the high data rates can be jeopardized due to the aforementioned mechanical hazards that they might be exposed to. In addition, the supervision of the physical layer of the network is fundamental because a break can cause the suspension of essential services, such as bank, telephone or internet services links. One way of discovering where a failure occurred in communications systems using fiber optics is to use a Rayleigh scatter-based monitoring system. There are some types of techniques that make use of this phenomenon, but what stands out most certainly is the Optical Time Domain Reflectometer (OTDR) (Barnoski et al., 1977). Through the use of an OTDR it is possible to extract information about the fiber's integrity by accessing only one end of the fiber, i.e., a central transmission station can monitor all the fibers connected to it without the need to install an apparatus for monitoring at each of the multiple nodes of the optical network. A good quality OTDR offers both good spatial resolution (less than 20 meters) and long range (greater than 200 kilometers) (Zhao et al., 2015).

The OTDR operates as follows: pulses of light, which are emitted periodically, are coupled to the test fiber through a circulator; the light pulses enter through port 1 of the circulator and exit through port 2 which is connected to the optical fiber under test; as these pulses propagate within the fiber a portion of the light is back-reflected due to Rayleigh scattering and Fresnel reflection; the backscattered light enters through port 2 of the circulator and is directed to port 3, which is connected to a photodetector; the electrical signal generated by the detector is sent to a microprocessor which calculates the round trip time,

Calliari, F., Herrera, L., Weid, J. and Amaral, G.
High-Dynamic and High-resolution Automatic Photon Counting OTDR for Optical Fiber Network Monitoring.
DOI: 10.5220/0006643900820090
In *Proceedings of the 6th International Conference on Photonics, Optics and Laser Technology (PHOTOPTICS 2018)*, pages 82-90
ISBN: 978-989-758-286-8

associates the backscattered power to a position in the fiber and produces an OTDR trace otherwise known as the fiber *profile*.

One of the most important parameters of an OTDR is the dynamic range, which is expressed in dB, and refers to the maximum length of an optical link that can be measured; it can also be understood as the maximum attenuation that can be measured in a optical fiber link. Another important parameter is the spatial resolution of the OTDR, which reflects the sensitivity to resolve two adjacent events. The spatial resolution depends mainly on the light pulse width entering the fiber. The greatest compromise relationship in OTDRs is between the dynamic range and spatial resolution since, in order to achieve higher resolution, narrow pulses are required, but, on ther other hand, the narrower the pulse, the less energy it will carry which results in a lower dynamic range (Agrawal, 1997).

1.1 Photon Counting OTDR

With the advent of the Geiger-mode Single Photon Detector (SPD) in the telecommunication wavelength, the Photon-Counting OTDR (ν-OTDR) was proposed. Such devices offer higher sensitivity due to extremely low power detection in the single-photon regime (Eraerds et al., 2010). Operating in the gated mode, such SPDs can attain high photon detection efficiencies and extremely low dark count rates (Eraerds et al., 2010). The gated operation requires, however, an intelligent management system to reduce monitoring periods and enhance the acquisition of statistically relevant data (Amaral et al., 2015).

The ν-OTDR can offer some advantages when compared to a conventional state-of-the-art OTDR, some of which include: higher spatial resolution, better dynamic range, better 2-point resolution, lower timing jitter and superior behavior concerning afterpulsing (Eraerds et al., 2010; Amaral, 2014). Of course, there are disadvantages too, some of which are: dead zones after large loss events (charge persistence effect); and trace speed, depending on the application (Herrera, 2015). Recently, a tunable ν-OTDR with 6 meters spatial resolution and 32 dB dynamic range has been proposed in a WDM-PON context (Amaral et al., 2014), herewith dubbed the High-Dynamic ν-OTDR, or HD-ν-OTDR. In (Herrera et al., 2015), the ν-OTDR is employed in a setup for ultra-high resolution measurements up to 3 centimeters with a 14 dB dynamic range, the Ultra-High Resolution ν-OTDR, or UHR-ν-OTDR.

2 MEASUREMENT ARRANGEMENT

In this work, the compromise relationship between dynamic range and spatial resolution has been tackled and a proposal for reducing the gap between the aforementioned prominent ν-OTDR techniques has been reached. The herewith described monitoring structure aims to unite the high dynamic range of the HD-ν-OTDR to the high resolution provided by the UHR-ν-OTDR with the objective of accurately and quickly finding faults in an optical fiber link. More importantly, the monitoring structure is fully automatic since an algorithm tailored for the application of finding faults in a fiber profile has been included. The chart shown in Fig. 1 shows the steps taken by the system to inspect a fiber optical link.

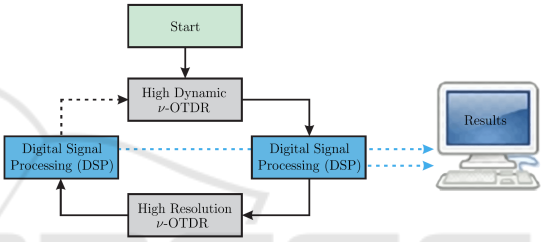

Figure 1: Flowchart of the Hybrid and Automatic ν-OTDR.

First, the system uses the HD-ν-OTDR to obtain a fiber profile whose resolution is ~ 6 m. Despite the limited resolution, the acquisition rate is quite high in a 20 km link, for example, the system allows the determination of the last point of the profile with a signal-to-noise ratio of 10 dB in just under two minutes (Amaral, 2014). Then the trend filter estimates the positions that may present faults and sends them as events list to the HR-ν-OTDR. The signal processing step is also quite accelerated, with extremely accurate results in just under a minute (Amaral et al., 2015). The HR-ν-OTDR, in turn, analyzes only the regions around the points of interest. Although the acquisition is time-consuming, the extremely significant reduction of the total fiber length to be inspected enables the results to be acquired with palatable times, in the order of minutes.

It is interesting, at this point, to explain the architectures of the different ν-OTDRs separately. However, in Fig. 2, the complete architecture of the proposal is presented. It should be noted that all components that originally belong to the HD-ν-OTDR architecture are above the SPD's line and, conversely, the components below the SPD's line are part of the HR-ν-OTDR architecture. In this architecture, all the devices that can be employed in both architectures are shared so that it is not only simplified but, also, occu-

pies less physical space.

In Fig. 2, the first Semiconductor Optical Amplifier (SOA), right after the Tunable Laser Source (TLS), boosts the optical signal inside a narrow window of 60 ns with a 2 A peak current driver creating high power narrow light pulses. The second SOA is driven by a 600 mA current pulse with 60 ns width. Even though the driving pulse is not enough to reach full power operation of the second SOA alone, the first boost guarantees optimal power usage while the second acted as a gainless optical switch, shaping the width of the optical pulse down to 60 ns. The tandem configuration of the SOAs guarantees a high extinction rate, contributing to the overall dynamic range of the detections. An FPGA is responsible for triggering a digital delay generator (DDG) which, in turn, triggers both of the SOA's drivers. The FPGA is also responsible for creating the gate pulses for the SPD; each detection is stored with its respective timing stamp and the data is transmitted through an USB cable from the FPGA to a computer. Wavelength tunability, in this setup, is guaranteed by the TLS.

In order to maximize the number of detections and reduce the acquisition time, a train of gates, spaced apart by the dead time of the SPD, is created (Wegmuller et al., 2004; Amaral, 2014). With every new light pulse that is sent into the optical fiber, a delay is added to the train of gates to ensure that the entire fiber is analyzed. The FPGA board is responsible for managing the train of gates and the delays between pulses as well as enabling the light pulses through the SOA's driver. This process is graphically detailed in Fig. 3 (Amaral et al., 2015). Each detection is associated with a 16 bit word – the time stamp – composed by r and s, the Gate and Pulse number, respectively. The parameters a, b and c represent the gate window, the dead time and the maximum delay between pulses.

Back to Fig. 2, we find, below the SPD line, the architecture of the UHR-ν-OTDR. The 115 fs wide pulses from an Ultra Wideband Laser Source (UWS) passes through a narrow bandpass filter and are then amplified by an Erbium Doped Fibre Amplifier (EDFA). The bandpass filter ensures that the EDFA will amplify only the selected wavelength and thus not wasting optical power. The tunability is guaranteed by the Tunable Filter which exhibits an ultrasharp roll-off ideal for Dense WDM (DWDM) monitoring. The pulses are, then, directed to an SOA which works as fast optical switch, reducing the pulse repetition rate and satisfy the condition of one light pulse traversing the fiber at a time. The enabling pulses of the SOA are generated by a DDG, which is triggered by the synchronizing signal from the UWS. These enabling pulses are reshaped by the SOA driver which is capable of driving the SOA with 4 ns-wide 600 mA pulses.

Since the light pulse passing through the SOA is 115 fs wide which is much narrower than 4 ns, the transmitted light pulse degrades due to the presence of amplified spontaneous emission (ASE) generated by the SOA. However, the corresponding ASE power is approximately 10 dB below the pulse peak and has little effect on the achievable spatial resolution of the technique (Herrera et al., 2016). The DDG also triggers the SPD with varying delays such as to cover the whole fiber length. Detections are processed by a Time-to-Digital Converter and sent to a computer. A Variable Optical Attenuator (VOA) at the SPAD's input guarantees that the power does not exceed the saturation limit so the detector is kept at linear regime (Eraerds et al., 2010). Wavelength tunability, in this setup, is achieved by the use of a narrow bandpass filter at the source's output (BPF).

It is evident from the schematic of Fig. 2 that the management system is essential for the architecture operation. It is responsible for interfacing with both ν-OTDRs and to processes the respective fiber profiles with the fault finding algorithm. It is also responsible for switching between the operation modes, which is accomplished by actuating upon the Optical and Radio-Frequency switches – OS and RFS in Fig. 2. The OS is responsible for injecting either the HD-ν-OTDR or the UHR-ν-OTDR pulse into the fiber while the RFS is responsible for directing the correct gate pulse to the SPD as they differ from one mode to the other (Amaral et al., 2015; Herrera et al., 2016).

3 RESULTS - LONG-DISTANCE FIBER LINK

A 36 km long fiber link composed of three almost identical fibers with 12 km each was used to generate the OTDR trace and the filtered signature shown in Fig. 4. The trend filter of choice for this work is the Adaptive ℓ_1 Filter, presented in (von der Weid et al., 2016), which has been shown to outperform several other signal processing techniques that focus on the identification of trends in data series. Depending on the size of the data series, the processing time can take from a few minutes to a few hours, which would be the case for a 36000 points data series. With the 6 meters bin, which corresponds to the spatial resolution of the HR-ν-OTDR, the approximately 36km fiber profile is represented by a $\sim$ 6000 points data series, so the Adaptive ℓ_1 Filter takes about two minutes to process the profile.

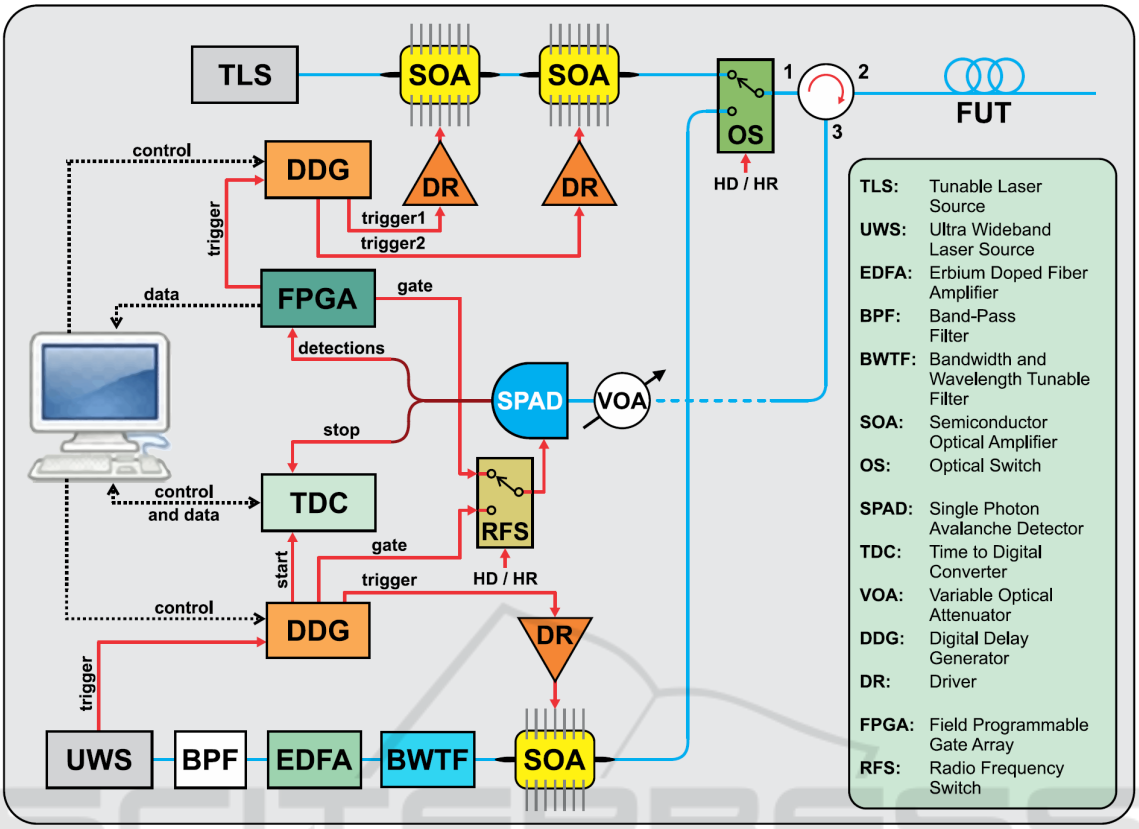

Figure 2: Architecture of the Hybrid and Automatic ν-OTDR for fast and accurate fault finding in optical fiber links.

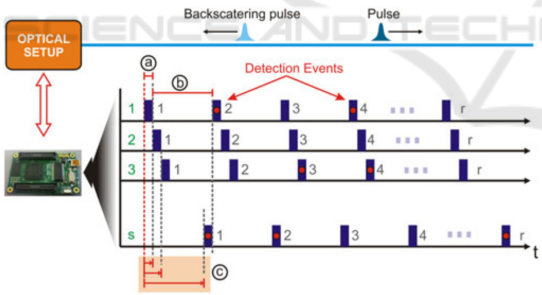

Figure 3: Graphical representation of the higher data acquisition method using the time-shifted train of gates in a single optical pulse (Amaral et al., 2015).

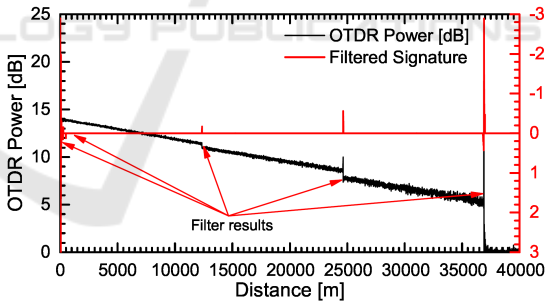

Figure 4: HD-ν-OTDR trace and the filtered signature of the ∼ 36km fiber link.

The output from the Adaptive ℓ_1 Filter is a list of events containing the location of candidates for fiber faults. The results were as follows: 0, 1011 ± 6, 12303 ± 6, 24603 ± 6 and 36830 ± 6 meters. It is evident that the beginning of the fiber is the first value of the list, which is neglected. It is noteworthy that the filter always selects the first positions, so it can be consistently neglected and is not an *ad hoc* procedure. The second value corresponds to a spurious detection and the rest corresponds to connectors and the fiber end.

According to the chart presented in Fig. 1, this list of events will be scrutinized with extreme resolution by the UHR-ν-OTDR; its role is both to determine whether the points correspond to actual faults and, in case it is indeed a fault, determine its position with higher resolution. The UHR-ν-OTDR is fed with the fault candidates positions and, also, with a spatial window (arbitrarily set as ± 100 meters) within which to search. The results of the UHR-ν-OTDR are shown in Figs. 5, 6, and 7.

Figs. 5 to 7 present the UHR-ν-OTDR monitoring results for the three actual faults in the link. It also

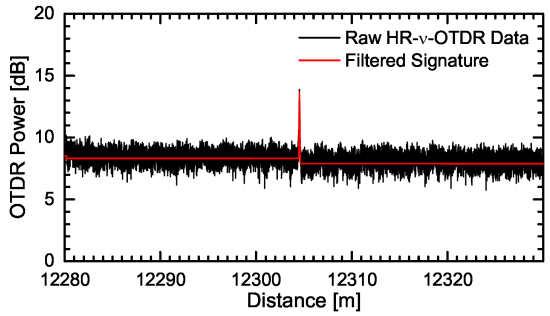

Figure 5: High-resolution measurement around 12303 ± 6 meters.

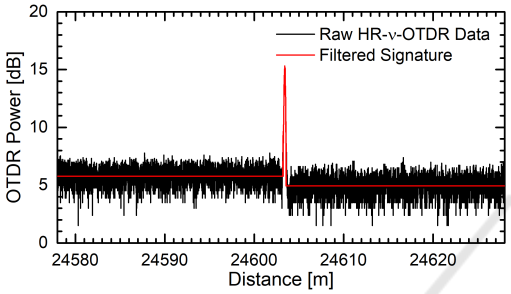

Figure 6: High-resolution measurement around 24603 ± 6 meters.

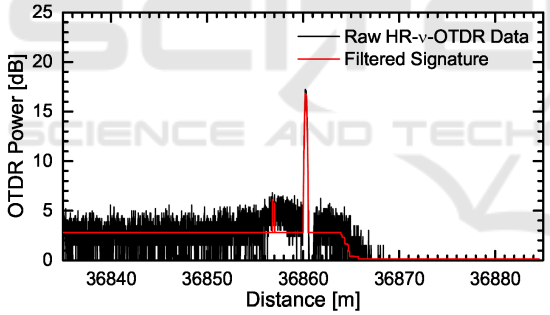

Figure 7: High-resolution measurement around 36830 ± 6 meters.

presents the detailed detection of the Adaptive ℓ_1 Filter, closing the last step of the chart presented in Fig. 1. The result of the 1011 ± 6 meters spurious detection is not presented, for simplicity. However, as expected, the Adaptive ℓ_1 Filter did not detect any trend break, which is interpreted as the absence of fault.

Overall, the whole procedure of determining, with precisions of up to 3cm, the fault positions of a 36km fiber has taken approximately 18 minutes where: 150 seconds correspond to the acquisition of the first profile with the HD-ν-OTDR; 150 seconds correspond to the processing step of the Adaptive ℓ_1 Filter that identifies potential fault candidates; 600 seconds correspond to the UHR-ν-OTDR measurements where each 200 meter stretch take one fourth of the whole time; and the final 300 seconds correspond to the time the Adaptive ℓ_1 Filter takes to process all of the high-resolution measurements, one fourth of the time per stretch.

4 RESULTS - MEDIUM-RANGE DWDM LINK

In order to evaluate the possibility of inspecting a wavelength-multiplexed link, link 2 was assembled containing a ∼2 km feeder fiber and two wavelength-dedicated fibers of ∼3.6 km and ∼12 km connected by a passive wavelength division multiplexer (WDM) at channels 37 and 40 of the DWDM grid. The results of the HD-ν-OTDR are presented in Figs. 8 and 9.

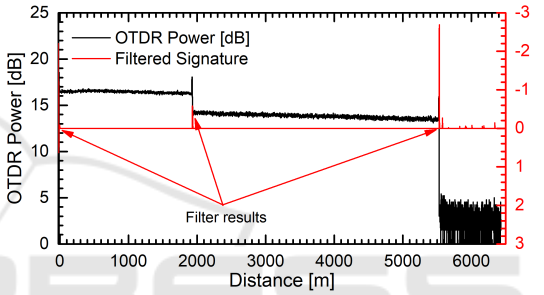

Figure 8: HD-ν-OTDR trace and the filtered signature of the $\sim 2 + 3.6$km fiber link at channel 37 of the DWDM grid.

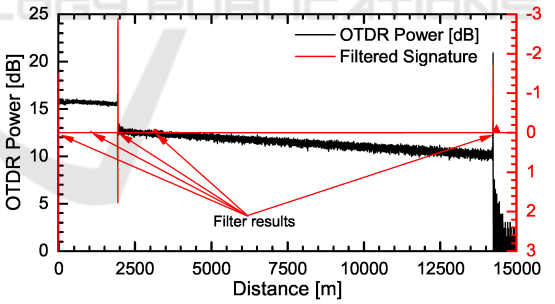

Figure 9: HD-ν-OTDR trace and the filtered signature of the $\sim 2 + 12$km fiber link at channel 40 of the DWDM grid.

Since both HD-ν-OTDR measurements (for channels 37 and 40) discovered a fault candidate at the same position (around 1948 ± 6 meters), we show, in Fig. 10, the high-resolution measurement result which is common for both measurements. Once again, we do not present the high-resolution measurement results for the spurious detections since, as expected, these have been discarded as fault positions after scrutiny of the UHR-ν-OTDR.

Apart from the WDM that connects the feeder fiber to the user fiber, no other faults were present at the measured links apart from the fiber ends. These

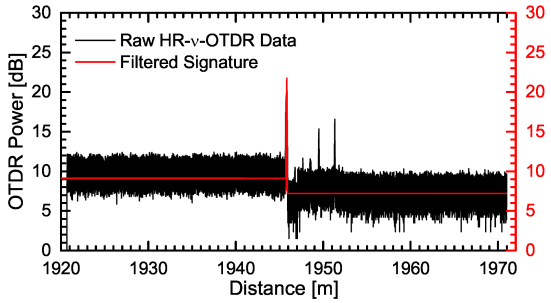

Figure 10: High-resolution measurement around 1945 ± 6 meters.

are presented in Fig. 11 and 12. The overall timing taken by the monitoring structure to return the high-resolution results for both links was approximately 25 minutes. It is clear that, even though the structure is robust against spurious detections in the first step, the impact is negative in the total timing. That is, of course, because each extra candidate scrutinized by the UHR-ν-OTDR translates into at least 3 extra minutes distributed between the data acquisition and the signal processing steps.

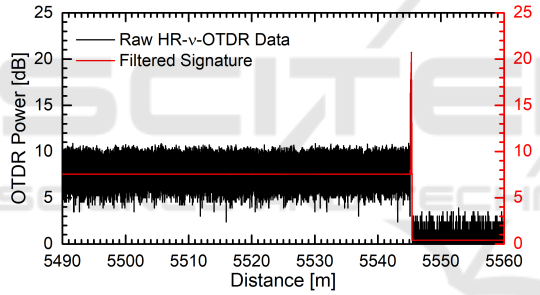

Figure 11: High-resolution measurement around 5525 ± 6 meters.

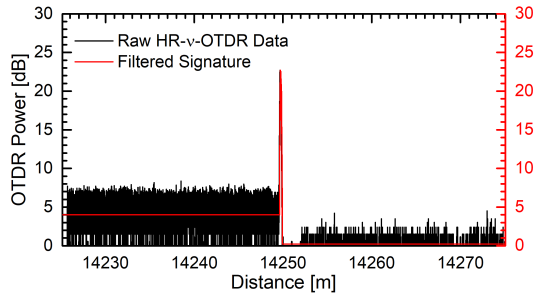

Figure 12: High-resolution measurement around 14250 ± 6 meters.

5 TUNABILITY, COHERENCE, CHROMATIC DISPERSION AND SPATIAL RESOLUTION

A tunable OTDR measurement compatible with WDM networks (as specified in ITUT G.694.1) must not only be capable of selecting the center wavelength of emission but also the spectral width of the optical signal. The current Dense WDM (DWDM) channels are either 0.8 nm wide comporting 40 channels or 0.4 nm wide comporting 80 channels, but devices that can operate with 0.2 nm wide channels (the so-called Ultra-Dense WDM) have already been proposed (Shahpari et al., 2015). The increasing number of channels will enable higher user capacity and more flexibility of the interconnections at the expense of reduced bandwidth per channel.

Compatibility between the probing pulse spectral shape and the network to be monitored becomes clear by the result of Fig. 13. In it, a broadband source was used to probe a WDM network composed by a feeder fiber, a WDM splitter and four user fibers. Since the source does not provide wavelength selectivity, the backscattered power from all the channels are overlapped and cannot be distinguished in the resulting profile except by the end-fiber reflection peak.

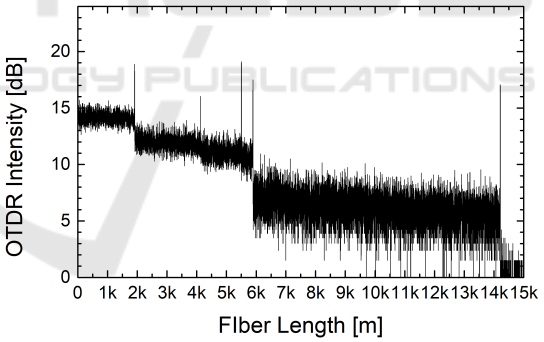

Figure 13: OTDR trace of a WDM network using the HD-ν-OTDR and a broadband light source. The overlapped profile does not allow for the distinction between each user fiber.

In Fig. 14, on the other hand, the profiles were acquired employing a spectrally-tailored optical source in order to meet the WDM channel's characteristics so that each individual user fiber could be probed individually. Evidently, more time needs to be spent in these measurements since each user fiber has to be monitored individually.

Recall that the pulse generated by the UWS for high-resolution inspection has an extremely broad spectrum and must be spectrally-tailored in order to fit the requirements of the WDM network it is applied to – see Section 2. At this point, two distinct effects

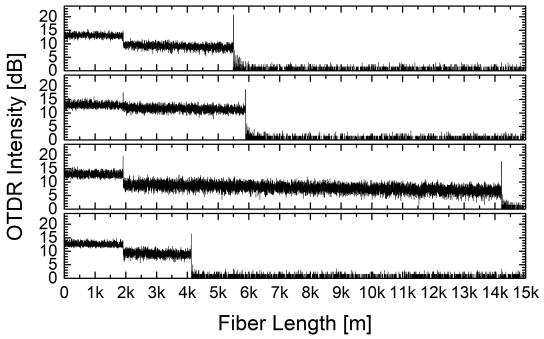

Figure 14: Individual OTDR traces using the HD-ν-OTDR for each of the user fibers. By spectrally-tailoring the optical signal, each user fiber can be individually addressed due to wavelength selectivity characteristics of WDM devices.

are in contrast: the coherent Rayleigh noise (CRN), which grows inversely proportional to the spectral width (De Souza, 2006); and the chromatic dispersion, which grows proportionally to the spectral width (Herrera et al., 2015). The CRN are the fluctuations in backscatter intensity due to the interference caused by the superposition of several light waves arriving at the detector with random phases (Shimizu et al., 1992).

Although the CRN arises due to the random distribution of the incoming wave phases, it cannot be averaged out with long-time measurements such as the counting noise (von der Weid et al., 2016). In order to illustrate the effect of the CRN on OTDR measurements, Fig. 15 presents two OTDR profiles of the same fiber – but using probe pulses with different line-widths: 600 kHz, the intrinsic linewidth of a tunable coherent laser; and 100GHz, a probe pulse spectrally-tairoled to match the 0.8 nm channel of DWDM-PONs (Caballero et al., 2013).

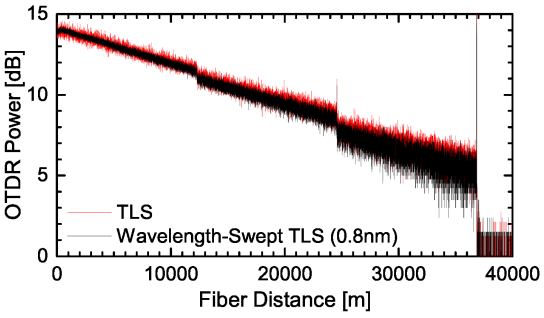

Figure 15: OTDR traces using the HD-ν-OTDR with two different spectral widths. The red trace, which has a much higher noise, was taken using a coherent laser with 600 kHz linewidth. The black trace was taken by employing a wavelength sweeping technique that mimics a broader linewidth (Caballero et al., 2013); for this, the same TLS was swept from 1554.13 to 1554.93 nm.

It becomes clear, thus, that, in order to avoid the presence of CRN in the OTDR profile, the probe pulse should be as spectrally broad as possible; in the specific case of WDM-PONs, the broader linewidth is the one that matches the whole channel bandwidth. Broadening the linewidth of the laser, however, will increase the time stretching of the optical pulse as it traverses the fiber due to chromatic dispersion (Elrefaie et al., 1988). Also, since the original emitted pulses are transform-limited, the spectral tailoring will have a direct impact on the time broadening. This condition constitutes a compromise relationship: if the optical pulse is spectrally-tailored to a narrow bandwidth, it will be enlarged in time and render poor spatial resolution in both short- and long-distance measurements; however, if the pulse is spectrally-tailored to the broader possible bandwidth value, the optical pulse will exhibit a good spatial resolution for short-distance measurements and, due to chromatic dispersion, a poor spatial resolution for long-distance measurements. This compromise relationship is translated in Fig. 16, where the achievable spatial resolution versus the bandwidth of the pulse is plotted for different fiber lengths. It is worth noting that, for each distance measurement, there is an optimal bandwidth value that corresponds to the best achievable spatial resolution. Also, detector's jitter may, sometimes, limit the spatial resolution instead of either the chromatic dispersion or the spectral width.

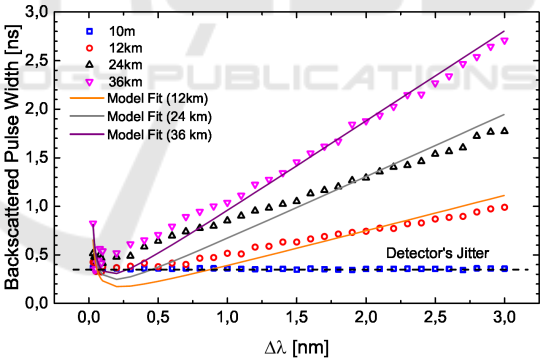

Figure 16: The compromise relationship between the spatial resolution and the spectral width for different fiber lengths. As expected, for longer fibers, broader bandwidths have a harsher impact on diminishing the achievable spatial resolution. In a 10 meter fiber, chromatic dispersion has negligible effect and the spatial resolution will be limited by the detector's jitter, as demonstrated by the blue dots.

The model used to fit the experimental data was the following:

$$W_p = \Delta\lambda \cdot a + \frac{b}{\Delta\lambda}, \quad (1)$$

where a corresponds to $2 \cdot \text{fiber length} \cdot D$ and b corresponds to pulse width of the UWS-1000H at full bandwidth, ie, $b \approx 20\,\text{fs} \cdot 800\,\text{nm}$. Also, we have used

an approximation for the dispersion factor D and assumed that it remained constant within $\Delta\lambda$. From the results, it is clear that slope for $\Delta\lambda \geq 1$ nm is well fitted, but the experimental results below this value show some inconsistencies with the fit. We conjecture that this behaviour may arise from the fact that the pulse peak power for reduced $\Delta\lambda$ is very low and the measurement results may be distorted. The back-reflected power also diminishes as the fiber length grows, which is observed in a higher contrast between experimental and fitted data for the longer fibers of 24.6 km and 32.8 km. The pulse width enlargement for low values of $\Delta\lambda$ is due to the transform-limited pulse, i.e., it is as short as its spectral bandwidth permits.

6 CONCLUSIONS

An automatic, highly accurate, and fast optical fiber link monitoring structure that aims to ally the best features of two distinct and prominent monitoring structures, namely the High-Dynamic and Ultra-High-Resolution Photon Counting OTDRs (Amaral et al., 2015; Herrera et al., 2015), has been successfully assembled. The fundamental constituent of the proposed architecture is a fault finding algorithm capable of accurately identifying fault candidates in a fiber profile. The employed algorithm enables the automation of the whole process so that an operator is no longer necessary to inspect each fiber profile, i.e., the results are output automatically. A video containing an experimental run of the method can be found in (Optoelectronics Laboratory – F. Calliari, L. E. Y. Herrera, J. P. von der Weid, and G. C. Amaral,).

The presented technology has been experimentally verified in long-range, mid-range, and wavelength multiplexed optical fiber links. The process involves four distinct steps: initially, a fast high-dynamic measurement is performed with the HD-ν-OTDR; next, the fiber profile is processed by the Adaptive ℓ_1 Filter and the fault candidates are identified; having the candidates list from the previous step, a high-resolution measurement is performed in the vicinity of the fault candidate position using the UHR-ν-OTDR; finally, the results of the previous step are also processed by the Adaptive ℓ_1 Filter and the actual fault positions are identified with extremely high accuracy. Our results show that faults in links as long as 36 km could be inspected with spatial resolutions of up to 3 cm in less than 15 minutes. This work paves the way for low-cost, highly reliable, automatic, and fast monitoring of optical fiber links.

ACKNOWLEDGMENT

The authors would like to thank brazilian agencies CNPq, Capes and FAPERJ for financial support.

REFERENCES

Agrawal, G. P. (1997). *Fiber-Optic Communication Systems*. John Wiley & Sons, Inc.

Amaral, G. C. (2014). FPGA Applications on Single Photon Detection Systems. Master's thesis, PUC-Rio.

Amaral, G. C., Garcia, J. D., Herrera, L. E., Temporao, G. P., Urban, P. J., and von der Weid, J. P. (2015). Automatic Fault Detection in WDM-PON with Tunable Photon Counting OTDR. *Journal of Lightwave Technology*, 33(24):5025–5031.

Amaral, G. C., Herrera, L. E., Vitoreti, D., Temporão, G. P., Urban, P. J., and der von Weid, J. P. (2014). WDM-PON monitoring with tunable photon counting OTDR. *IEEE Photonics Technology Letters*, 26(13):1279–1282.

Barnoski, M. K., Rourke, M. D., Jensen, S. M., and Melville, R. T. (1977). Optical Time Domain Reflectometer. *Applied Optics*, 16(9):2375–2379.

Caballero, D. V., von der Weid, J., and Urban, P. (2013). Tuneable otdr measurements for wdm-pon monitoring. In *Microwave & Optoelectronics Conference (IMOC), 2013 SBMO/IEEE MTT-S International*, pages 1–5. IEEE.

De Souza, K. (2006). Significance of coherent rayleigh noise in fibre-optic distributed temperature sensing based on spontaneous brillouin scattering. *Measurement Science and Technology*, 17(5):1065.

Elrefaie, A. F., Wagner, R. E., Atlas, D., and Daut, D. (1988). Chromatic dispersion limitations in coherent lightwave transmission systems. *Journal of Lightwave Technology*, 6(5):704–709.

Eraerds, P., Legré, M., Zhang, J., Zbinden, H., and Gisin, N. (2010). Photon Counting OTDR: Advantages and Limitations. *Journal of Lightwave Technology*, 28(6):952–964.

Herrera, L., Amaral, G., and von der Weid, J. P. (2015). Ultra-high-resolution tunable pc-otdr for pon monitoring in avionics. In *Optical Fiber Communications Conference and Exhibition (OFC), 2015*, pages 1–3. IEEE.

Herrera, L. E., Calliari, F., Garcia, J. D., do Amaral, G. C., and von der Weid, J. P. (2016). High Resolution Automatic Fault Detection in a Fiber Optic Link via Photon Counting OTDR. In *Optical Fiber Communication Conference*, page M3F.4. Optical Society of America.

Herrera, L. E. Y. (2015). *Reflectometria óptica de alta resolução por contagem de fótons*. PhD thesis, PUC-Rio.

Optoelectronics Laboratory – F. Calliari, L. E. Y. Herrera, J. P. von der Weid, and G. C. Amaral. Higy-dynamic and high-resolution automatic photon counting otdr. `https://www.youtube.com/watch?v=KQn9Du2l4NQ&feature=youtu.be`.

Shahpari, A., Ferreira, R., Ribeiro, V., Sousa, A., Ziaie, S., Tavares, A., Vujicic, Z., Guiomar, F. P., Reis, J. D., Pinto, A. N., et al. (2015). Coherent ultra dense wavelength division multiplexing passive optical networks. *Optical Fiber Technology*, 26:100–107.

Shimizu, K., Horiguchi, T., and Koyamada, Y. (1992). Characteristics and reduction of coherent fading noise in rayleigh backscattering measurement for optical fibers and components. *Journal of Lightwave Technology*, 10(7):982–987.

von der Weid, J. P., Souto, M. H., Garcia, J. D., and Amaral, G. C. (2016). Adaptive filter for automatic identification of multiple faults in a noisy otdr profile. *Journal of Lightwave Technology*, 34(14):3418–3424.

Wegmuller, M., Scholder, F., and Gisin, N. (2004). Photon-counting otdr for local birefringence and fault analysis in the metro environment. *Journal of lightwave technology*, 22(2):390–400.

Zhao, Q., Xia, L., Wan, C., Hu, J., Jia, T., Gu, M., Zhang, L., Kang, L., Chen, J., Zhang, X., et al. (2015). Long-haul and high-resolution optical time domain reflectometry using superconducting nanowire single-photon detectors. *Scientific reports*, 5:10441.